Research Article

Mamduh J. Aljaafreh*, and Rageh. K. Hussein

# Substituent effect on the electronic and optical properties of newly designed pyrrole derivatives using density functional theory

https://doi.org/10.1515/phys-2024-0012
received November 23, 2023; accepted March 25, 2024

**Abstract:** This work explores six newly designed compounds obtained by several substitutions in 2,5-di(2-thienyl) pyrrole molecule. For this series of compounds, the electronic and optical properties were investigated using density functional theory and time-dependent density functional theory (TD-DFT). The new compounds were characterized by calculating the chemical parameters that correlated with their optical and electrical properties. The lowest unoccupied molecular orbital (LUMO) and the highest occupied molecular orbital (HOMO) energies are calculated using the B3LYP functional with the 6-311G (d, p) basis set. The most low-lying energy level of the LUMO was found for Perr-$NO_2$, indicating its effective electron injection capabilities and oxidation resistance. The HOMO and LUMO distributions of Perr-Cl and Perr-$NO_2$ displayed a remarkable complementarity throughout each component of the two compounds, indicating an effective intermolecular charge transfer. The molecular electrostatic potential analysis demonstrated that the proposed compounds have a broad distribution of electrophilic and nucleophilic sites, which predict a high degree of chemical reactivity. The electron density analysis at the bonding and anti-bonding sites of the title compounds was performed using the electron localization function and local orbital locator techniques. Noncovalent interaction analysis using the reduced density gradient approach classified all types of interaction: repulsive, weak, and attractive interactions within compound fragments. All compounds exhibited a robust repulsive interaction, as proved by the red spikes at 0.038 a.u. The ultraviolet/visible (UV/vis) spectrum was obtained by TD-DFT using CAM-B3LYP models in conjunction with 6-311G (d, p) basis set and methanol as a solvent, the absorption bands were found within the UV range, and the maximum wavelength showed red-shifted increases. These compounds could serve as a base material for developing selective gas sensors with considerable UV/vis absorption (180–400 nm). According to the research results, the designed compounds are good candidates for use as precursors in polymer designs for optoelectronic and sensor applications due to their high electrical conductivity and photochemical properties.

**Keywords:** pyrroles, DFT/TD-DFT, frontier molecular orbitals, UV/vis spectra, optoelectronic and sensing properties

## 1 Introduction

The pyrrole and thiophene systems have significance due to their remarkably high reactivity among the various types of polymers displaying electroconductive characteristics. This significance comes from the presence of condensed poly-heterocyclic units that retain an extended conjugated C═C structure. Many years ago, scientists studied polymers that could be converted into conductive materials by pyrolysis or, substituent effects, or any other means. The investigation and development of many conjugated polymers (CPs) were inspired by the discovery of the high conductivity of doped polyacetylene [1–3]. Since then, CPs have been regarded as a promising material for developing electronic components due to their potential as organic conductors [4,5]. One structural feature all CPs share is the poly-conjugation in the π-system of their backbone. Many different approaches have been employed in the search for improved CPs. These approaches included chemical modifications such as selective sulfur oxidation, ring fusion, substitution by other heteroatoms, and elongation of the chain [6–8]. Polymers containing pyrrole/thiophene rings are attractive for producing materials with high conductive properties. Within these two categories (pyrrole/thiophene), the ability to modify the β-position of the pyrrole ring and the free α-positions of thiophene

* **Corresponding author: Mamduh J. Aljaafreh,** Department of Physics, College of Science, Imam Mohammad Ibn Saud Islamic University (IMSIU), Riyadh, 11623, Saudi Arabia, e-mail: maljaafreh@imamu.edu.sa
**Rageh. K. Hussein:** Department of Physics, College of Science, Imam Mohammad Ibn Saud Islamic University (IMSIU), Riyadh, 11623, Saudi Arabia

rings provide further controlling and tuning of their properties [9–11]. Alkyl groups are frequently used as substituents in the β-position of pyrrole or thiophene rings. The resultant polymers exhibit the advantage of improved processing because of their increased solubility in organic solvents [12]. The electrical and optical properties of such materials are mainly determined by the structure of the starting monomer, which is strongly affected by the substituents' steric and electronic properties [13,14]. Scientists and researchers are becoming interested in these polymers because of their potential applications in different scientific and technological fields, such as sensors, batteries, electrocatalysts, electrochromic devices, the synthesis of new materials, and electrophotography [15–19]. A new electroactive derivative of 2,5-di(2-thienyl)pyrrole was synthesized by Soganci *et al.,* leading to produce a novel solution-processable and fluorescent polymer called poly (*N*-(2,5-di(thiophen-2-yl)-1*H*-pyrrol-1-yl)-3,4,5-tris(dodecyloxy) benzamide) (P(TPDOB)) [20].

The newly synthesized 2,5-di(2-thienyl)pyrrole derivative, 4-amino-*N*-(2,5-di(thiophen-2-yl)-1*H*-pyrrol-1-yl) benzamide (HKCN) was achieved through the reaction between 1,4-di(2-thienyl)-1,4-butanedione and *p*-aminobenzoyl hydrazide. HKCN exhibits excellent stability compared to other 2,5-di(2-thienyl)pyrrole derivatives and retains a lower band gap, indicating improved conductivity [21].

Recent work by Altun *et al.* was mainly focused on the development of biosensing interfaces applied benzenamine-2,5-di(thienyl)pyrrole (SNS-An) and 3,4-ethylenedioxythiophene (EDOT) in a copolymerization technique. The P (SNS-An) and P(SNS-An-co-EDOT) films were prepared and cross-linked with glucose oxidase and supplemented with carbon nano-elements to improve their biosensing properties. The P(SNS-An-co-EDOT) film demonstrated superior performance compared to the P(SNS-An) film in terms of analytical characteristics and recovery rate accuracy [22].

Conjugated pyrrole materials also have the attractive features of readily available and simple synthesis processes. The chemical synthesis of pyrrole polymers has an extensive record [23]. The chemical oxidative polymerization with ferric chloride acting as an oxidant in aqueous media has been widely used to produce pyrroles; this procedure is simple and reasonably of low cost [24–26]. Several techniques could be used to carry out this process, depending on the oxidant and solvent types. It has been reported that different oxidants, such as halogens and organic electron acceptors, are used to synthesize pyrroles, along with different solvents, such as water and chloroform [27,28]. Recently, it has been reported that CuH-catalyzed enyne–nitrile coupling is an effective reaction to synthesize substituted pyrroles [29].

It was a common challenge to obtain reliable physical data to characterize and analyze extended π-chain polymers with high molecular weight and structural defects [30,31]. Therefore, theoretical approaches were used to obtain reliable supporting information for the molecular, chemical, and physical properties of the polymer structure. Density functional theory (DFT) and time-dependent density functional theory (TD-DFT) are two of the most well-known and widely used theoretical techniques for studying molecular geometry and structural features related to the chemical and physical properties of materials [32–36]. The compound cyclohexylammonium perchlorate $(C_6H_{14}N)ClO_4$ was synthesized and characterized using experimental and computational methods. DFT calculations were made at the B3LYP/6-311+ +G(d,p) level. The highest occupied molecular orbital (HOMO), lowest unoccupied molecular orbital (LUMO), and gap energy orbital analyses were used to determine the electronic properties of the compound [37]. Another study investigated urea–water mixtures using DFT and experimental methods, with a reduced density gradient (RDG) analysis and non-covalent interaction (NCI). In addition, for urea–water combinations with different molar urea fractions, experimental infrared spectra were obtained. The harmonic vibrational frequencies of urea–$(H_2O)_n$ complexes were calculated theoretically using the B3LYP method with a 6-311G++(d, p) basis set [38].

The DFT approach is also widely recognized for designing, characterizing, and improving the performance of pyrrole–thiophene-based polymers [39–41].

This research aims to study the effects of substituent groups on the electronic and optical properties of a modified 2,5-di(2-thienyl) pyrrole molecule. Six new molecules were designed from this molecule by substituting different donating/withdrawing groups with the hydrogen bonded to the nitrogen of the pyrrole ring. DFT-Becke–Lee–Yang–Parr's three-parameter hybrid functional (B3LYP) with Pople's triple zeta 6-311G (d, p) basis set investigations were accomplished to analyze the electronic properties associated with the optimized structure for each compound. Many analyses of the ground-state optimized structure were carried out using molecular electrostatic potentials along with frontier molecular orbital and associated quantum chemical parameters to comprehend reactivity and intermolecular charge transfer. NCI was implemented to analyze the different types of interactions within the studied compounds. The UV/vis spectra and associated photochemical properties were simulated and analyzed using TD-DFT with CAM-B3LYP models in conjunction with the 6-311G (d, p) basis set. The simulations were performed in the presence of methanol as a solvent.

# 2 Materials and methods

## 2.1 Chemistry and molecular design

Highly electro-conductive materials are an ongoing research focus to keep up with modern optoelectronic applications. The pyrrole and thiophene ring system provides extremely reactive molecules with the ability to incorporate substituents at different positions along their rings. 2,5-Di(2-thienyl) pyrroles, consisting of thiophene and pyrrole rings, are of great interest due to their potential for generating substantially electro-conductive derivatives. Prior research on the reactivity of 2,5-di(2-thienyl) pyrroles produced condensed poly-heterocyclic compounds by substituting in the β-position of the pyrrole ring and also in α-positions of thiophene rings [42]. In that work, 2,5-di(2-thienyl) pyrroles (shown in Figure 1a) were subjected to several substitution processes with the modified components to produce 16 new products. In addition to their electro-conductive capabilities, these poly-heterocyclic compounds with extended C═C conjugated systems are expected to be promising structural fragments of photochromic dihetarylethenes. One of the substitution processes described in the cited study was a series of synthesis procedures that yielded what we will term “base compound” (Figure 1b). The base compound received a dimethyl substitution to produce a compound that was named 2,6-dimethyl-1,3,5,7-tetrakis(5-methyl-2-thienyl)-4,8-dihydropyrrolo[3,4-*e*] benzo[b]pyrrole; details of its synthesis are also provided in the quoted work. New pyrrole derivatives have been designed by substituting various functional groups at the di-substitution sites R in the base compound. The basic compound has been designated by the acronym Perr, and the functional group (R) was added after that acronym has been used to denote the new derivatives, specifying the substituents R = $CH_3$, $NH_2$, OH, $OCH_3$, Cl, and $NO_2$, respectively, and the new derivatives, namely, Perr-$CH_3$, Perr-$NH_2$, Perr-OH, Perr-$OCH_3$, Perr-Cl, and Perr-$NO_2$ respectively.

## 2.2 Computational methods

The ground-state energies associated with the optimized structures were calculated using the Gaussian 09W program [43]. The level of the used DFT was based on the model B3LYP with a 6-311G (d, p) basis set [44]. Many research works have shown that DFT calculations using the B3LYP functional in combination with the 6-311++G (d,p) basis set can perfectly predict molecular structures that are consistent with experimental results [37,45].

Many parameters, such as HOMO and LUMO frontier molecular orbitals, their corresponding energy levels, and molecular electrostatic potential, have been visualized using the advanced molecular visualizer Avogadro software [46]. The TD-DFT was used to simulate UV/vis spectra. In that context, modeling excited-state attributes using the conventional B3LYP functional has been realized to have considerable drawbacks. The new hybrid exchange-correlation functional, known as the Coulomb-attenuating method (CAM-B3LYP), was developed to address these issues. To more effectively account for the long-range effects of electron–electron interactions in excited states, the Coulomb-attenuating approach, which is included in CAM-B3LYP, was selected for this investigation [47]. Multiwfn was used for the calculation of electron localization function (ELF), local orbital locator (LOL), and NCI-RDG [41,48]. The visual molecular dynamics (VMD) tool was used to display the charts and color maps more accurately [49].

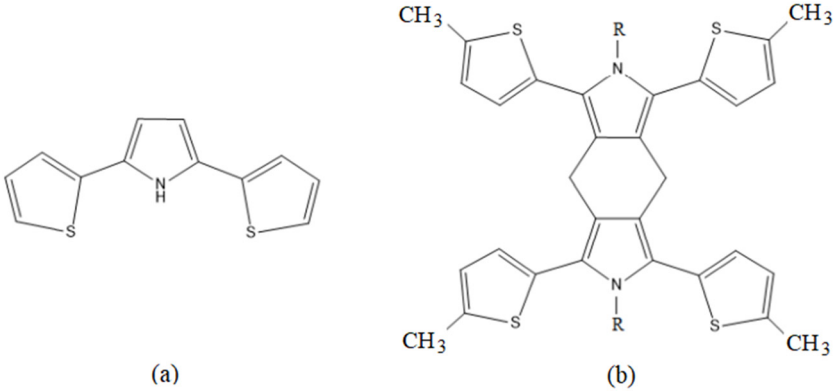


**Figure 1:** (a) 2,5-Di(2-thienyl) pyrrole compound and (b) the base compound was the building block for creating the new derivative, R = $CH_3$, $NH_2$, OH, $OCH_3$, Cl, and $NO_2$, respectively.

# 3 Results and discussion

The concept of frontier molecular orbitals is commonly employed to study the reactivity of most chemical compounds, mainly HOMO and LUMO. The HOMO–LUMO energy gaps, together with some other chemical parameters, are well known to be important in understanding the optical and electrical properties of materials. The molecular electrical properties of a molecule can be determined by the HOMO–LUMO energy gap ($\Delta E$); a molecule with a low HOMO–LUMO energy gap has a high degree of chemical reactivity.

It has been observed that there is a direct correlation between the stability of the compound and its hardness ($\eta$), as well as its reactivity and softness ($\sigma$). Compounds with high $\eta$ have greater stability and lower reactivity, while those with high $\sigma$ are more reactive and less stable. When undergoing a chemical reaction, a compound can also be described as hard, less reactive, and more stable, or soft, more reactive, and least stable. These two classifications can be identified by the parameters $\eta$ and $\sigma$, respectively. The ability of an atom or molecule to draw electrons to itself is referred to as electronegativity ($\chi$) in chemical terms. The electrophilicity index ($\omega$) quantifies the energy stabilization that occurs when a system accepts an additional electron from its surroundings. These parameters were derived using Koopmans' theorem, which developed a theoretical method for utilizing the electronic properties of a system to predict the corresponding chemical activity [50]. Table 1 presents all the equations used to calculate $\Delta E = E_{\mathrm{LUMO}} - E_{\mathrm{HOMO}}$, and $\eta$, $\sigma$, and $\chi$ were calculated by using the equations listed as follows:

**Table 1:** All the equations used to calculate HOMO–LUMO energy gap along with its associated quantum chemical parameters for designed pyrrole derivatives

| | |
|---|---|
| $\Delta E = E_{\mathrm{LUMO}} - E_{\mathrm{HOMO}},$ | (1) |
| $\eta = -\frac{(E_{\mathrm{HOMO}} - E_{\mathrm{LUMO}})}{2},$ | (2) |
| $\sigma = \frac{1}{\eta},$ | (3) |
| $\chi = -\frac{(E_{\mathrm{HOMO}} + E_{\mathrm{LUMO}})}{2},$ | (4) |
| $\omega = \frac{\chi^2}{2\eta}.$ | (5) |

A list of the calculated data used as a chemical reactivity descriptor is shown in Table 2. The table shows that Perr-$NO_2$ is the most reactive compound because it has the lowest energy gap value. As a result of having the largest energy gap, Perr-$CH_3$ was the most stable of all the studied compounds. In line with the previous findings, the Perr-$NO_2$ compound was found to have the lowest hardness/highest softness value and Perr-$CH_3$ has the opposite behavior. The highest value of electronegativity, which is a sign of significant charge flow, was observed for Perr-$NO_2$. Perr-$NO_2$ was identified as having an electrophilic nature and high energy stabilization when accepting an electron pair since it showed the highest electrophilicity value ($\omega$ = 4.74 eV). The previous findings show that the substitution of the $NO_2$ group on the base compound considerably increased its chemical reactivity and provided it with excellent electro-conductive properties.

The variation of HOMO and LUMO energy levels has a major effect on photovoltaic properties such as light absorption, intermolecular charge transfer, and charge extraction/injection. Increases in the HOMO and LUMO energy levels can be attributed to electron-donating functional groups by adding more electrons to the system, causing an increase in electron–electron repulsion. On the other hand, electron-withdrawing groups remove electrons, which can work to lower the HOMO and LUMO energy levels. One form of reaction that has a detrimental effect on electron transport within electroconductive materials is electrochemical oxidation for the excited electrons delocalized within the LUMO. To prevent this kind of interaction, the LUMO energy level must be sufficiently low/deep, or the electron affinity must be sufficiently high [51]. Figure 2 depicts the HOMO and LUMO energy levels of the studied pyrrole derivatives. As seen in the figure, the electron-donating group $NH_2$ was found to have the highest level of HOMO in Perr-$NH_2$, while Perr-$CH_3$ displayed the

**Table 2:** HOMO–LUMO energy gap and its associated quantum chemical parameters for designed pyrrole derivatives

| Compounds | $E_{\mathrm{HOMO}}$ (eV) | $E_{\mathrm{LUMO}}$ (eV) | $\Delta E$ (eV) | $\eta$ (eV) | $\sigma$ $(\mathrm{eV})^{-1}$ | $\chi$ (eV) | $\omega$ (eV) |
|---|---|---|---|---|---|---|---|
| Perr-$CH_3$ | −4.869 | −0.968 | 3.901 | 1.951 | 0.51 | 2.919 | 2.18 |
| Per-$NH_2$ | −4.737 | −1.152 | 3.585 | 1.793 | 0.56 | 2.945 | 2.42 |
| Perr-OH | −4.766 | −1.278 | 3.488 | 1.744 | 0.57 | 3.022 | 2.62 |
| Perr-$OCH_3$ | −4.739 | −1.232 | 3.507 | 1.753 | 0.57 | 2.986 | 2.54 |
| Perr-Cl | −5.208 | −1.598 | 3.61 | 1.805 | 0.55 | 3.403 | 3.21 |
| Perr-$NO_2$ | −5.631 | −2.308 | 3.323 | 1.662 | 0.60 | 3.970 | 4.74 |

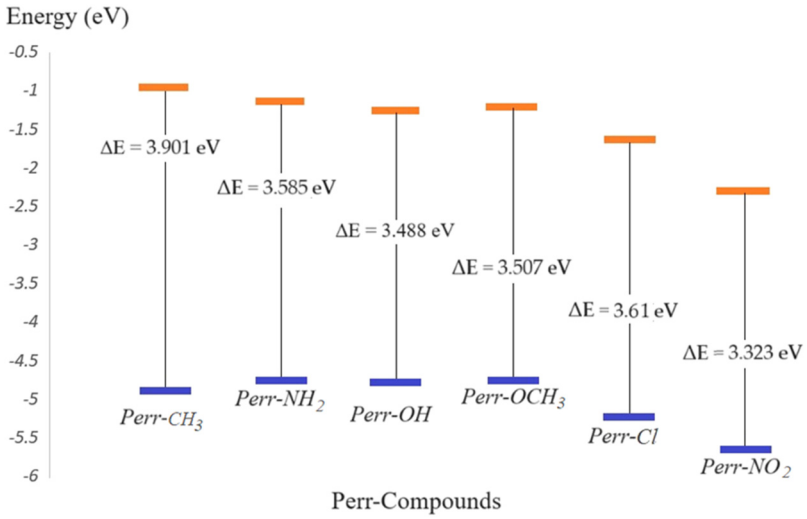


**Figure 2:** Positions of the HOMO and LUMO energy levels of the designed pyrrole derivatives on the energy scale.

highest level of LUMO. Compared to other derivatives, the HOMO and LUMO levels dropped to their lowest levels as a result of the electron-withdrawing $NO_2$ group. This result would provide the Perr-$NO_2$ compound with more effective electron injection capabilities and oxidation resistance.

Based on the contributions of the frontier molecular orbital and their HOMO/LUMO distribution along the skeleton of the molecule, the intermolecular charge transfer activity could be predicted. HOMO represents the electron donor orbitals, while LUMO represents the electron acceptors orbitals, and they are scaling for the ionization potential and the electron affinity, respectively. The contour plots in Figure 3 demonstrate that HOMO and LUMO orbitals are dispersed along the whole conjugated framework and share a common style for most derivatives. The thiophene and methyl groups in Perr-Cl and Perr-$NO_2$ do not form LUMO orbitals in contrast to the other derivatives due to the strong electron-withdrawing Cl and $NO_2$ groups. The HOMO orbitals have a bonding feature within each unit fragment. The LUMO orbitals reveal an anti-bonding characteristic inside every component and a bonding characteristic between the two neighboring fragments. The substituent groups have no contribution in HOMO orbitals; the same effect is seen in LUMO except for Perr-Cl and Perr-$NO_2$, where the functional groups have bonding orbitals with the nitrogen of the pyrrole ring. There is a fully conjugated distribution of HOMO and LUMO orbitals on the central bridge ring, which provide an effective charge transfer between the upper and lower 2,5-di(2-thienyl) pyrrole chains. Both Perr-Cl and Perr-$NO_2$ compounds prominently display the latter effect by having a huge LUMO lobe across the central ring. There is a perfect complementarity between the HOMO and LUMO contribution within each unit in Perr-Cl and Perr-$NO_2$, which indicates a strong intermolecular charge transfer within the two compounds.

The molecular electrostatic potential (MEP) is the net electrostatic behavior caused by the total charge distribution at the surface of a molecule. MEP describes the chemical activities of molecules in their interactions with other chemical species. In MEP, different electrostatic potential values are denoted by different colors. Blue and red are color combinations that represent positive and negative MEP regions, respectively, while the neutral electrostatic potential is symbolized by the color white. The positive electrostatic potential region is a prospective site for the attack of electron-rich species (nucleophilic attack). In contrast, the negative electrostatic potential region is a potential position for the attack of electron-deficient species (electrophilic attacks). Figure 4 displays the MEP surfaces of all the investigated pyrrole derivatives. The nitrogen of the pyrrole ring is where all payroll compounds have their negative electrostatic potential regions. The oxygen atom in the Perr-OH and Perr-$OCH_3$ surpassed the nitrogen of the pyrrole ring as the spots with the most negative electrostatic potential. The Perr-Cl and Perr-$NO_2$ groups have a slightly negative electrostatic potential due to a smaller proportion of negative charge. All of the aforementioned locations constitute the prime targets for electrophilic attacks. On the other hand, the hydrogen atoms of methyl groups and the hydrogen atoms of the central carbon atoms are sources of positive electrostatic potential. The largest positive potential zones were found to be on the hydrogens of the hydroxyl and amine groups, as well as, to a lesser extent, on the hydrogens of the methoxy group. These locations could potentially act as sites for the nucleophilic attack.

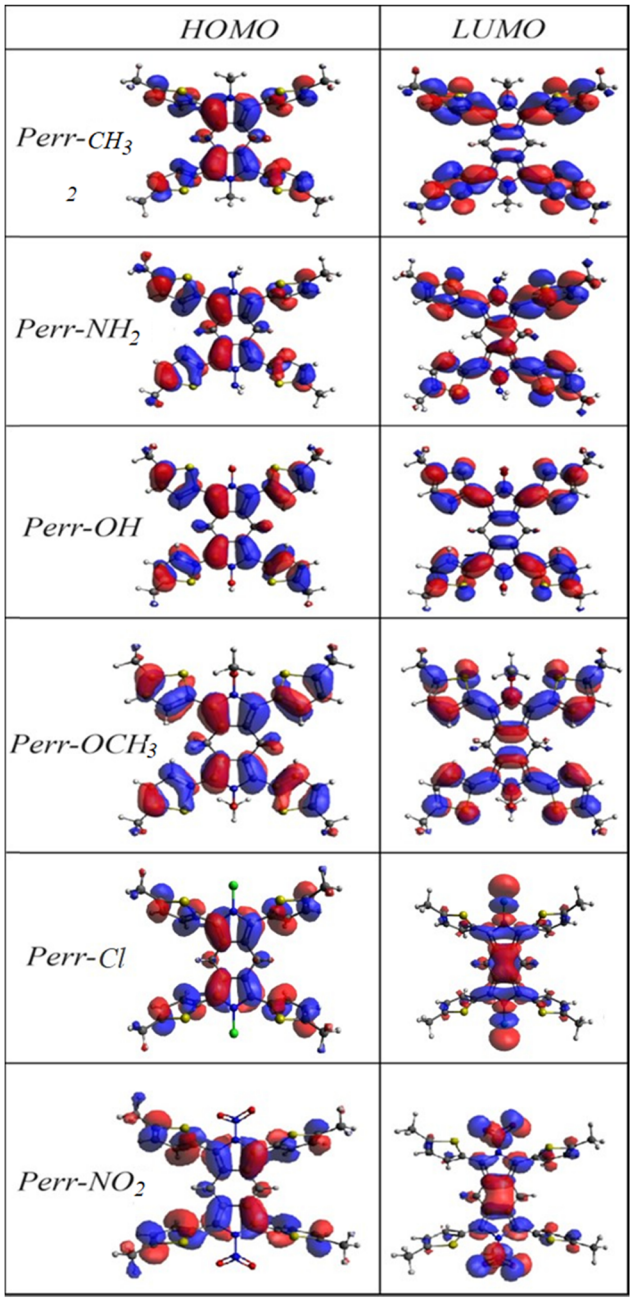


**Figure 3:** Distribution of HOMO and LUMO frontier molecular orbitals of all the derivatives under investigation.

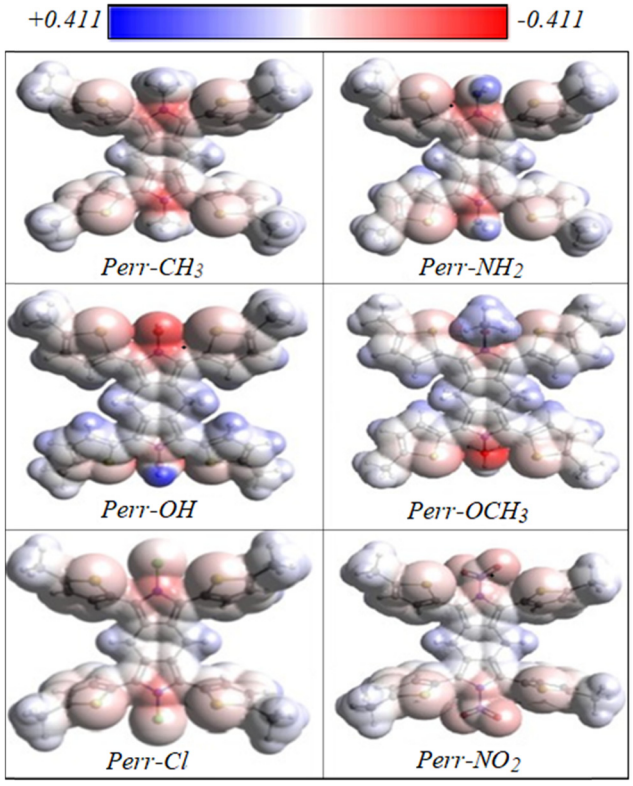


**Figure 4:** Maps of MEP of all the derivatives under investigation.

A common technique for describing the electronic environment of an atom and classifying chemical bonds is the surface analysis of the ELF and the LOL. ELF has been identified based on the electron pair density, and LOL is used to represent a gradient of localized orbitals where localized orbitals overlap [52]. The ELF map was constructed within the range of 0.0 to 1.0, with the region representing the bonding and non-bonding localized electrons falling between 0.5 and 1.0 (red color) and the delocalized electrons represented by smaller values <0.5 (blue color). The LOL is a simple manner of the ELF, with the distinction that its values are in the range from 0 to 0.8. The formation of a covalent bond involving a lone pair or inner shells of an atom, which denote highly localized electrons, is indicated by a large value of LOL or red color. The contour color maps that depict the ELF and LOL patterns of the pyrrole derivatives are shown in Figures 5 and 6. A localized electron cloud interaction is shown by the high value of the red region surrounding the hydrogen atoms. The last two compounds, Perr-Cl and Perr-$NO_2$, exhibited a noticeable drop in the intensity of the red color, which could be a result from the stronger withdrawing groups, Cl and $NO_2$. The delocalized electron clouds surrounding some carbon atoms in the studied compounds can be seen in blue areas, which implies that these regions of the compound are the potential sites of interactions with other molecules or atoms. The covalent locations (high LOL value/red color) between the carbon and hydrogen atoms were slightly found in Perr-$CH_3$ and Perr-$NH_2$, increased in Perr-OH and Perr-$OCH_3$, and limited to the thiophene ring in Perr-Cl and Perr-$NO_2$. The red and blue colors of Perr-OH and Perr-$OCH_3$ were equally distributed, indicating a combination of bonding and non-bonding electrons, whereas the terminals and core carbon rings of Perr-Cl and Perr-

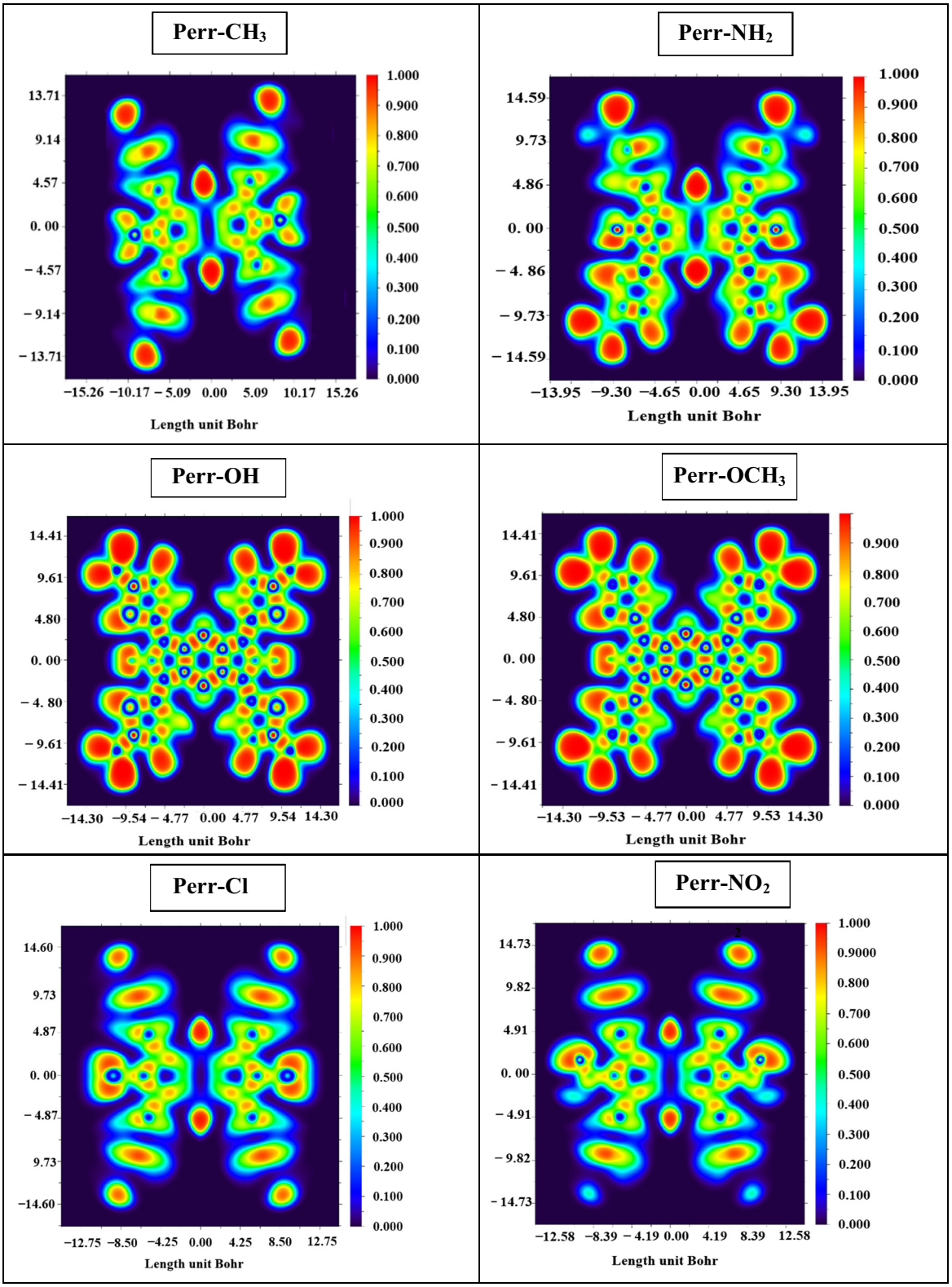


**Figure 5:** ELF contour maps for the studied pyrrole derivatives.

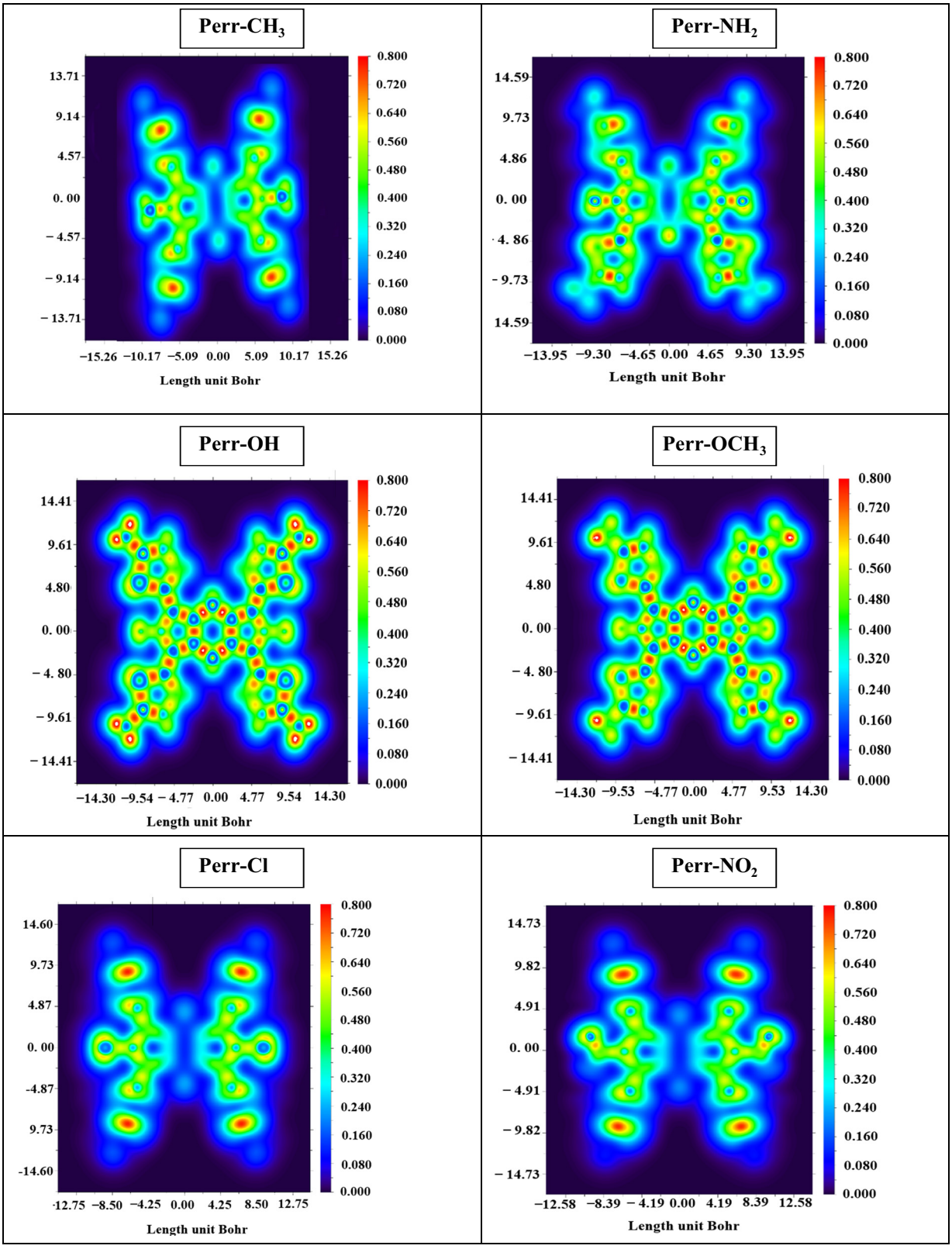


**Figure 6:** LOL contour maps for the studied pyrrole derivatives.

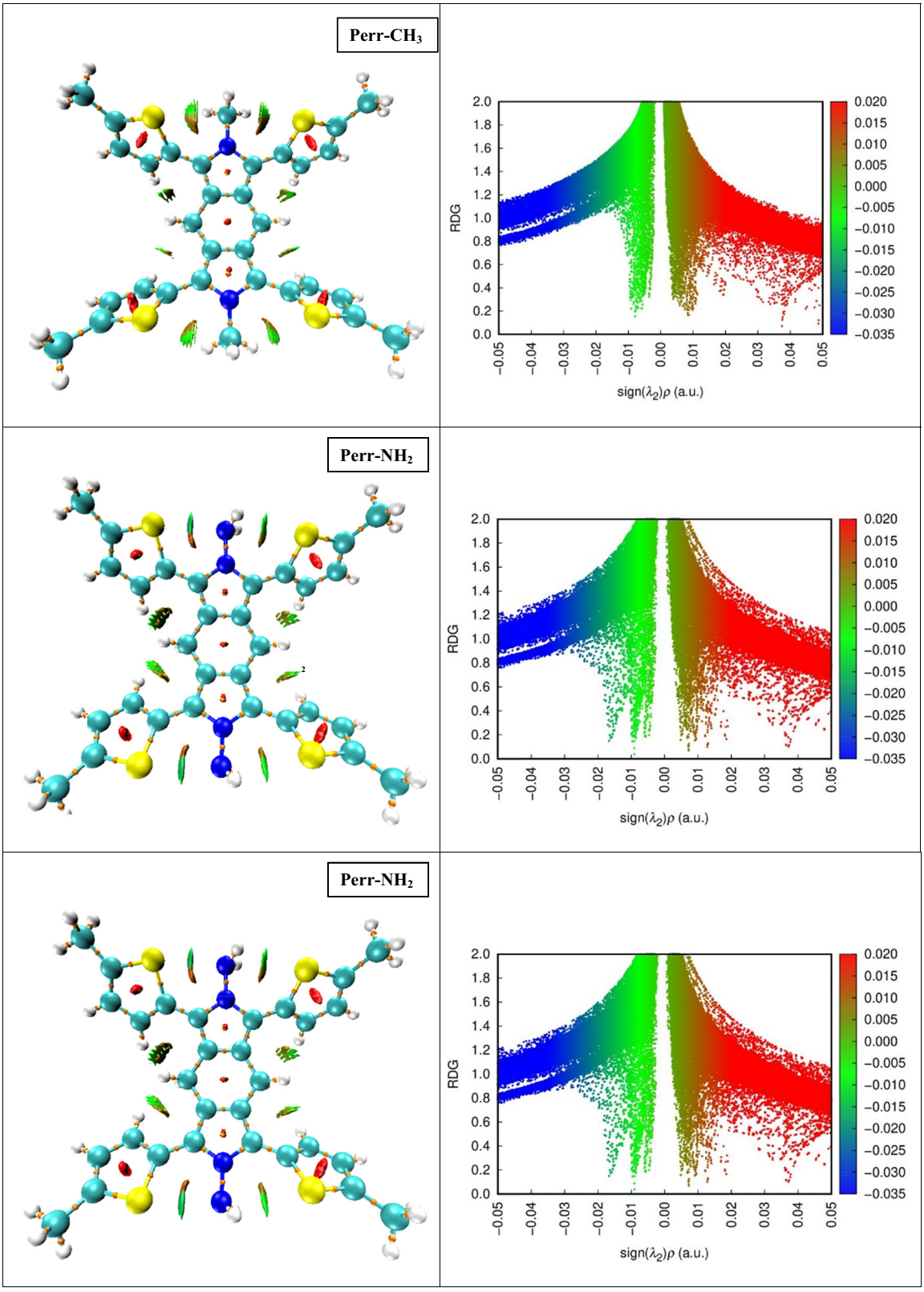


**Figure 7:** Plots of NCI (left) and RDG (right) for Perr-$CH_3$, Perr-$NH_2$, and Perr-OH derivatives.

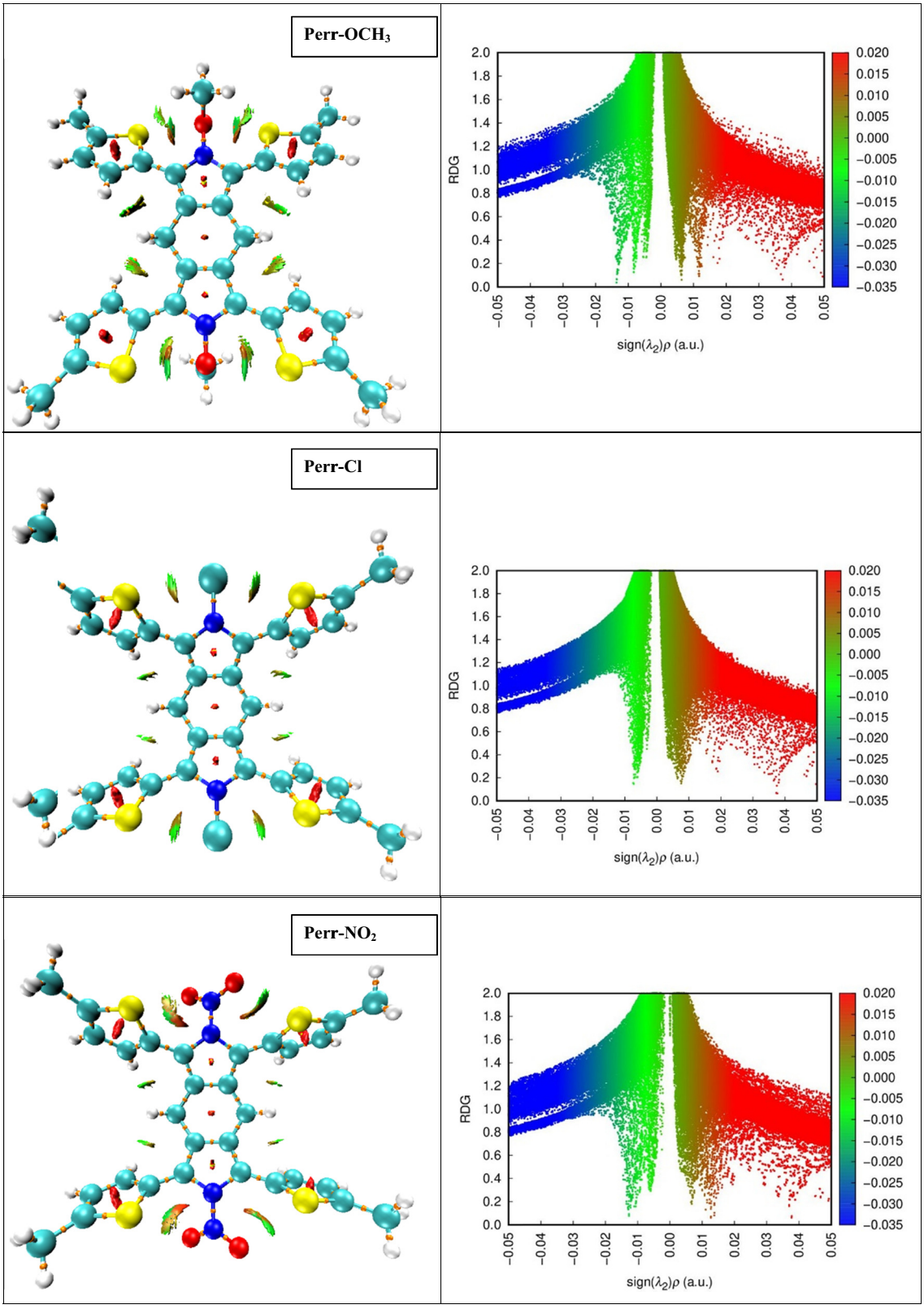


**Figure 8:** Plots of NCI (left) and RDG (right) for Perr-$OCH_3$, Perr-Cl, and Perr-$NO_2$ derivatives.

**Table 3:** Values of the product $(\lambda_2)\rho$ to distinguish the types of interactions for all the derivatives under investigation

| Compounds | Repulsive interactions sign $(\lambda_2)\rho > 0$ | Weak interactions sign $(\lambda_2)\rho \approx 0$ | Attractive interactions sign $(\lambda_2)\rho > 0$ |
|---|---|---|---|
| Perr-$CH_3$ | — | −0.0079 | 0.038 |
| Per-$NH_2$ | −0.017 | −0.0092 | 0.038 |
| | | | 0.013 |
| Perr-OH | −0.015 | −0.0094 | 0.038 |
| | | | 0.018 |
| Perr-$OCH_3$ | −0.013 | −0.0080 | 0.038 |
| | | | 0.012 |
| Perr-Cl | — | −0.0074 | 0.038 |
| Perr-$NO_2$ | −0.013 | — | 0.038 |
| | | | 0.013 |

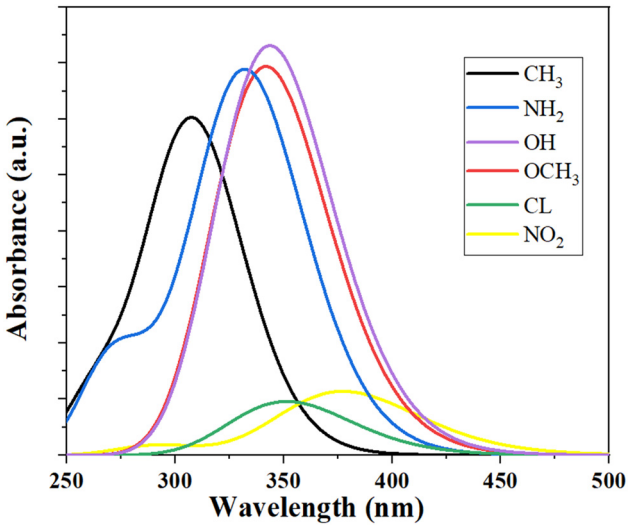


**Figure 9:** Simulated UV/vis absorption spectra of the studied pyrrole derivatives.

$NO_2$ exhibited a high concentration of delocalized electrons, as demonstrated by the blue color.

The analysis of NCI is facilitated by the efficient approach known as RDG, which investigates electron density and its derivatives in real space [53]. In both small molecules and molecular complexes, RDG can be used to distinguish between steric repulsion, van der Waals interactions, and hydrogen bonds. Multiplying the electron density ($\rho$) by the sign of the second eigenvalue $\lambda_2$ is a recommended method for distinguishing between different kinds of interactions. The three types of interactions that can be distinguished based on the product of $(\lambda_2)\rho$ are attractive interactions, such as hydrogen bonds or dipole–dipole interactions, indicated by negative values of $(\lambda_2)\rho$; nonbinding interactions of a repulsive nature, indicated by large positive values of the sign $(\lambda_2)\rho$; and weak interactions, like van der Waals interactions, where $(\lambda_2)\rho$ values are close to zero. The strength of the interaction is indicated via graphs that plot RDG versus $(\lambda_2)\rho$ values. The strong attraction is shown by large negative values of sign $(\lambda_2)\rho$ (blue color), the very weak interaction is marked with values closer to zero (green color), and the repulsive interaction is shown by large positive values (red color). The plots of NCI and RPG iso-surfaces are shown in Figures 7 and 8, and the values of sign $(\lambda_2)\rho$ are collected in Table 3. The small blue, green, and red colored patches on the NCI plot aid in understanding the various types of interactions according to the location of the lowest spikes (dashed points) on the horizontal scale of the RDG plot. According to the figure analysis, all derivatives have strong (steric) repulsive interactions at 0.038 a.u (red color), mainly located at the centers of the thiophene and pyrrole rings. A patch with a mixture of the three colors between the thiophene rings and the substituent groups represents the three types of interactions. A small attractive interaction is observed clearly at −0.017, and −0.015 a.u. in Perr-$NH_2$ and Perr-OH, and −0.013 a.u. for both Perr-$OCH_3$ and Perr-$NO_2$. All of the compounds exhibit the van der Waals interaction, with the exception of $NO_2$. There is also a small steric repulsion (light brown) at 0.013, 0.018, 0.012, and 0.013 a.u.,

**Table 4:** Calculated wavelength, excitation energies, oscillator strengths, and main transition associated with each UV band for the studied pyrrole derivatives

| Compounds | Wavelength (nm) | Energy (eV) | Oscillator strength | Transition | Major contribution |
|---|---|---|---|---|---|
| Perr-$CH_3$ | 308.403 | 4.02 | 1.461 | HOMO → LUMO | 88% |
| Perr-$NH_2$ | 332.370 | 3.730 | 1.684 | HOMO → LUMO | 66% |
| | 273.689 | 4.530 | 0.477 | HOMO → L + 2 | 30% |
| Perr-OH | 343.617 | 3.608 | 1.806 | HOMO → LUMO | 91% |
| Perr-$OCH_3$ | 341.837 | 3.627 | 1.713 | HOMO → LUMO | 76% |
| Perr-Cl | 351.349 | 3.528 | 0.237 | HOMO → LUMO | 69% |
| Perr-$NO_2$ | 377.345 | 3.286 | 0.2751 | HOMO → LUMO | 60% |
| | 292.243 | 4.242 | 0.044 | H-1 → LUMO | 36% |

respectively. Finally, the mixed color spikes between the thiophene and center rings imply C–H..... π interaction.

### 3.1 UV/vis spectrum

One intrinsic photophysical property of molecules is the UV/vis spectrum, which is produced when light is absorbed by electrons that are excited to higher energy levels. The potential of a molecule to readily oxidize could be regarded as a fundamental characteristic for predicting its reactivity; this property corresponds to a high UV absorption wavelength. Figure 9 displays the stimulated absorption spectra of pyrrole-modified compounds with their associated data reported in Table 4. Each derivative displays a single-absorption peak, which corresponds to a HOMO-to-LUMO electronic transition, except for Perr-$NH_2$ and $NO_2$, which have additional peaks related to HOMO → L + 2 and H-1 → LUMO, respectively. Red-shifted increases were observed in the calculated maximum wavelength as the substituent groups moved on from $CH_3$ to $NO_2$, according to the legend chart included in the figure, with a small exception that Perr-$OCH_3$ has a slightly smaller wavelength than Perr-OH. The increased $\lambda_{max}$ in that order may be due to the stronger electron-withdrawing capacity order for the substituent. Perr-$NO_2$ has the highest maximum wavelength value, revealing the high conductivity in interaction, which is compatible with its low energy gap value. Finally, absorption bands were found within the UV region ($\lambda_{max}$ ≈ 292 to 377 nm). Several derivatives of 2,5-di(2-thienyl)pyrrole materials exhibit a similar behavior in terms of their absorption spectra [54–56]. Several gas molecules exhibit high absorption in the UV/vis (180–400 nm); hence, a selective sensor framework can be developed by exploiting the absorption properties of these compounds.

## 4 Conclusions

Six pyrrole–thiophene compounds were designed based on the 2,5-di(2-thienyl) pyrrole molecule to attain high optoelectronic and sensing properties. The results showed that the Perr-$NO_2$ molecule exhibited the lowest LUMO energy level, indicating its effective electron injection capabilities and oxidation resistance. The Perr-Cl and Perr-$NO_2$ compounds exhibited complementary HOMO and LUMO distributions, suggesting effective intermolecular charge transfer, which reveals their dispersion over the entire conjugated backbone with bonding and anti-bonding characteristics. The chemical reactivity was evaluated by determining reactivity descriptors such as hardness, softness, electrophilicity, and electronegativity. Perr-$NO_2$ was found to have the lowest hardness, highest softness, and highest electronegativity and electrophilicity.

MEP was used to define the compounds' electrophilic and nucleophilic regions in order to figure out how it interacted with other molecules. The theoretical UV/vis spectra showed absorption bands in the UV range associated with the π–π* transition, and the maximum wavelength exhibited red-shifted increases. This proposes that the compounds could be used as base materials to develop selective sensors for gases with UV/vis absorption properties. These results are predicted to be important for further research into the types of the studied compounds to tailor a highly effective functional device.

**Funding information:** The authors extend their appreciation to the Deputyship for Research & Innovation, Ministry of Education in Saudi Arabia for funding this research through the project number IFP-IMSIU-2023121. The authors also appreciate the Deanship of Scientific Research at Imam Mohammad Ibn Saud Islamic University (IMSIU) for supporting and supervising this project.

**Author contributions:** Mamduh J. Aljaafreh and Rageh. K. Hussein: conceptualization, methodology, investigation, data curation, writing – original draft, formal analysis, software, and writing – review and editing. All authors have accepted responsibility for the entire content of this manuscript and approved its submission.

**Conflict of interest:** The authors state no conflict of interest.

**Data availability statement:** The datasets generated and/or analyzed during the current study are available from the corresponding author on reasonable request.

## References

[1] Guo X, Facchetti A. The journey of conducting polymers from discovery to application. Nat Mater. 2020;19:922–8.
[2] Namsheer K, Rout CS. Conducting polymers: A comprehensive review on recent advances in synthesis, properties and applications. RSC Adv. 2021;11:5659–97.
[3] Feast WJ, Tsibouklis J, Pouwer KL, Groenendaal L, Meijer EW. Synthesis, processing and material properties of conjugated polymers. Polymer (Guildf). 1996;37:5017–47.
[4] Anguera G, Sánchez-García D. Conjugated polymers: Synthesis and applications in optoelectronics. Afinidad. 2014;71:251–62.
[5] Al-Azzawi AGS, Aziz SB, Dannoun EMA, Iraqi A, Nofal MM, Murad AR, et al. A mini review on the development of conjugated polymers: Steps towards the commercialization of organic solar cells. Polymers (Basel). 2022;15:164.

[6] Mutlu H, Theato P. Making the best of polymers with sulfur–nitrogen bonds: From sources to innovative materials. Macromol Rapid Commun. 2020;41:2000181.
[7] Infante Teixeira L, Landfester K, Thérien-Aubin H. Selective oxidation of polysulfide latexes to produce polysulfoxide and polysulfone in a waterborne environment. Macromolecules. 2021;54:3659–67.
[8] Andriianova AN, Biglova YN, Mustafin AG. Effect of structural factors on the physicochemical properties of functionalized polyanilines. RSC Adv. 2020;10:7468–91.
[9] Apetrei R-M, Camurlu P. Functional platforms for (bio) sensing: Thiophene-pyrrole hybrid polymers. J Electrochem Soc. 2020;167:37557.
[10] Wetzel C, Brier E, Vogt A, Mishra A, Mena-Osteritz E, Bäuerle P. Fused thiophene-pyrrole-containing ring systems up to a heterodecacene. Angew Chem Int Ed. 2015;54:12334–8.
[11] Shah AUHA, Ullah S, Bilal S, Rahman G, Seema H. Reduced graphene oxide/poly (pyrrole-co-thiophene) hybrid composite materials: Synthesis, characterization, and supercapacitive properties. Polymers (Basel). 2020;12:1110.
[12] Tat'yana VV, Efimov ON. Polypyrrole: A conducting polymer; its synthesis, properties and applications. Russ Chem Rev. 1997;66:443.
[13] Farinola GM, Babudri F, Cardone A, Hassan Omar O, Naso F. Synthesis of substituted conjugated polymers: Tuning properties by functionalization. Pure Appl Chem. 2008;80:1735–46.
[14] Hawks AM, Altman D, Faddis R, Wagner EM, Bell K-JJ, Charland-Martin A, et al. Relating design and optoelectronic properties of 1, 4-dihydropyrrolo [3, 2-b] pyrroles bearing biphenyl substituents. J Phys Chem B. 2023;127:7352–60.
[15] Deshpande SD. Structure and properties of conducting polymers incorporated with phthalocyanine. PhD thesis. India: Pune University; 2000.
[16] Sarswat PK, Sathyapalan A, Zhu Y, Free ML. Design, synthesis, and characterization of TPA-thiophene-based amide or imine functionalized molecule for potential optoelectronic devices. J Theor Appl Phys. 2013;7:1–9.
[17] Cao X, Min Y, Tian H, Liu J. Incorporating cyano groups to a conjugated polymer based on double B ← N-bridged bipyridine units for unipolar n-type organic field-effect transistors. Org Mater. 2021;3:469–76.
[18] Mirabedini A, Foroughi J, Wallace GG. Developments in conducting polymer fibres: From established spinning methods toward advanced applications. RSC Adv. 2016;6:44687–716.
[19] Subramani NK, Siddaramaiah MR, Lee JH. Polymer-based advanced functional composites for optoelectronic and energy applications. Amsterdam, The Netherlands: Elsevier; 2021. ISBN 0128185090.
[20] Soganci T, Soyleyici HC, Ak M. A soluble and fluorescent new type thienylpyrrole based conjugated polymer: Optical, electrical and electrochemical properties. Phys Chem Chem Phys. 2016;18:14401–7.
[21] Söyleyici HC, Ak M, Şahin Y, Demikol DO, Timur S. New class of 2, 5-Di (2-thienyl) pyrrole compounds and novel optical properties of its conducting polymer. Mater Chem Phys. 2013;142:303–10.
[22] Altun A, Apetrei R-M, Camurlu P. The effect of copolymerization and carbon nanoelements on the performance of poly (2, 5-Di (thienyl) pyrrole) biosensors. Mater Sci Eng C. 2019;105:110069.
[23] Arrieta Almario AA, Tarazona Caceres RL. Study of kinetic formation and the electrochemical behavior of polypyrrole films. J Chil Chem Soc. 2009;54:14–9.
[24] Chitte HK, Shinde GN, Bhat NV, Walunj VE. Synthesis of polypyrrole using ferric chloride (FeCl3) as oxidant together with some dopants for use in gas sensors. J Sens Technol. 2011;1:47.
[25] Fadel M, Fadeel DA, Ibrahim M, Hathout RM, El-Kholy AI. One-step synthesis of polypyrrole-coated gold nanoparticles for use as a photothermally active nano-system. Int J Nanomed. 2020;15:2605–15.
[26] González J, Fernández AJ, Otero TF. Tailored synthesis of polypyrroles. Electronics and optical properties of conjugated molecular systems in condensed phases. Research Signpost, Kerala; 2003. p. 123–52.
[27] Heck J, Goding J, Lara RP, Green R. The influence of physicochemical properties on the processibility of conducting polymers: A bioelectronics perspective. Acta Biomater. 2022;139:259–79.
[28] Brandner L, Müller TJJ. Multicomponent synthesis of chromophores–The one-pot approach to functional π-systems. Front Chem. 2023;11:1124209.
[29] Zhou Y, Zhou L, Jesikiewicz LT, Liu P, Buchwald SL. Synthesis of pyrroles through the CuH-catalyzed coupling of enynes and nitriles. J Am Chem Soc. 2020;142:9908–14.
[30] Qin L, Zhao N, Sha Y, Chen H, Li L, Zhou D, et al. Characterization of conformational transition of polymers with low molecular weights in solutions by fluorescence resonance energy transfer. Polymer (Guildf). 2020;190:122217.
[31] Schmid F. Understanding and modeling polymers: The challenge of multiple scales. ACS Polym Au. 2022;3:28–58.
[32] Hussein RK, Bashter II, El-Okr M, Ibrahim MA. DFT investigation of structural and electronic properties of modified PZT. Acta Chem Iasi. 2019;27:15–30.
[33] Hussein RK, El-Khayatt AM, Alkaoud AM, Khouqeer GA, Deghady AM. Covalent inhibition for SARS-CoV-2 M pro via zinc ion transported by hydroxychloroquine: Investigated by DFT, ADMET and molecular docking. 2023;13(5):460.
[34] Aljaafreh MJ, Prasad S, AlSalhi MS, Alahmed ZA, Al-Mogren MM. Optically pumped intensive light amplification from a blue oligomer. Polymers. 2019;11(10):1534. doi: 10.3390/polym11101534.
[35] Aljaafreh MJ, Prasad S, AlSalhi MS, Alhandel RH, Alsaigh RA. TD-DFT simulation and experimental studies of a mirrorless lasing of poly [(9, 9-dioctylfluorenyl-2, 7-diyl)-co-(1, 4-diphenylene-vinylene-2-methoxy-5-{2-ethylhexyloxy}-benzene)]. Polymers (Basel). 2021;13:1430.
[36] Mhadhbi N, Issaoui N, Hamadou WS, Alam JM, Elhadi AS, Adnan M, et al. Physico-chemical properties, pharmacokinetics, molecular docking and in-vitro pharmacological study of a cobalt (II) complex based on 2-aminopyridine. ChemistrySelect. 2022;7:e202103592.
[37] Daghar C, Issaoui N, Roisnel T, Dorcet V, Marouani H. Empirical and computational studies on newly synthesis cyclohexylammonium perchlorate. J Mol Struct. 2021;1230:129820.
[38] Hammami F, Issaoui N, Nasr S. Investigation of hydrogen bonded structure of urea-water mixtures through infra-red spectroscopy and non-covalent interaction (NCI) theoretical approach. Comput Theor Chem. 2021;1199:113218.
[39] Akram SJ, Hadia NMA, Shawky AM, Iqbal J, Khan MI, Alatawi NS, et al. Designing of thiophene [3, 2-b] pyrrole ring-based NFAs for high-performance electron transport materials: A DFT study. ACS Omega. 2023;8:11118–37.
[40] Ahmed S, Dutta R, Kalita DJ. Strategical designing of diketopyrrolopyrrole-thiophene based donor-acceptor type organic oligomers and study their transport properties: A DFT/TD-DFT perspective. Chem Phys Lett. 2019;730:14–25.
[41] Wei W, Ren W, Jian W, Xia B, Zhang H, Bai F-Q, et al. Stability, aromaticity, and photophysical behaviors of macrocyclic molecules: A theoretical analysis. Front Chem. 2020;8:776.
[42] Belen'Kii LI, Gromova GP, Smirnov VI. Reactions of 2, 5-di (2-thienyl) pyrroles. Chem Heterocycl Compd. 2008;44:1092–100.

[43] Frisch MJ, Trucks GW, Schlegel HB, Scuseria GE, Robb MA, Cheeseman JR, et al. Gaussian 09, Revision D. 01. Wallingford CT: Gaussian, Inc.; 2009. See also http//www.gaussian.com.
[44] Yang Y, Weaver MN, Merz KM Jr. Assessment of the "6-31 + G** + LANL2DZ" mixed basis set coupled with density functional theory methods and the effective core potential: Prediction of heats of formation and ionization potentials for first-row-transition-metal complexes. J Phys Chem A. 2009;113:9843–51.
[45] Kazachenko AS, Medimagh M, Issaoui N, Al-Dossary O, Wojcik MJ, Kazachenko AS, et al. Sulfamic acid/water complexes (SAA-H2O (1-8)) intermolecular hydrogen bond interactions: FTIR, X-ray, DFT and AIM analysis. J Mol Struct. 2022;1265:133394.
[46] Hanwell MD, Curtis DE, Lonie DC, Vandermeersch T, Zurek E, Hutchison GR. Avogadro: An advanced semantic chemical editor, visualization, and analysis platform. J Cheminform. 2012;4:1–17.
[47] Martynov AG, Mack J, May AK, Nyokong T, Gorbunova YG, Tsivadze AY. Methodological survey of simplified TD-DFT methods for fast and accurate interpretation of UV–Vis–NIR spectra of phthalocyanines. ACS Omega. 2019;4:7265–84.
[48] Lu T, Chen F. Multiwfn: A multifunctional wavefunction analyzer. J Comput Chem. 2012;33:580–92.
[49] Humphrey W, Dalke A, Schulten K. VMD: Visual molecular dynamics. J Mol Graph. 1996;14:33–8.
[50] Terayama K, Osaki Y, Fujita T, Tamura R, Naito M, Tsuda K, et al. Koopmans' theorem-compliant long-range corrected (KTLC) density functional mediated by black-box optimization and data-driven prediction for organic molecules. J Chem Theory Comput. 2023;19:6770–81.
[51] Lüder J, Manzhos S. First-principle insights into molecular design for high-voltage organic electrode materials for Mg based batteries. Front Chem. 2020;8:83.
[52] Chamorro E. A complementary view to the bonding pattern in the N5 + cation: An electron localization function and local temperature analysis. J Chil Chem Soc. 2003;48:63–7.
[53] Wu P, Chaudret R, Hu X, Yang W. Noncovalent interaction analysis in fluctuating environments. J Chem Theory Comput. 2013;9: 2226–34.
[54] Tamilavan V, Sakthivel P, Li Y, Song M, Kim C, Jin S, et al. Synthesis and characterization of indenofluorene-based copolymers containing 2, 5-bis (2-thienyl)-N-arylpyrrole for bulk heterojunction solar cells and polymer light-emitting diodes. J Polym Sci Part A Polym Chem. 2010;48:3169–77.
[55] Pandule SS, Shisodia SU, Pawar RP, Chabukswar VV. Synthesis, properties, and ammonia gas sensing applications of poly-[1-(4-nitronaphthalen-1-Yl)-2, 5-di (thiophen-2-Yl)-1 H-pyrrole]. Polym Plast Technol Eng. 2017;56:268–75.
[56] Koyuncu S, Zafer C, Sefer E, Koyuncu FB, Demic S, Kaya İ, et al. A new conducting polymer of 2, 5-bis (2-thienyl)-1H-(pyrrole)(SNS) containing carbazole subunit: Electrochemical, optical and electrochromic properties. Synth Met. 2009;159:2013–21.